Catalysis Letters Vol. 102, Nos. 3–4, August 2005 (© 2005)
DOI: 10.1007/s10562-005-5871-5

Gold supported CeO_2/Al_2O_3 catalysts for CO oxidation: influence of the ceria phase

Miguel Ángel Centeno*, Cristina Portales, Ignacio Carrizosa, and José Antonio Odriozola

Institute de Ciencia de Materiales de Sevilla, Centro Mixto CSIC-Universidad de Sevilla, Avda Americo Vespuccio s/n, 41092 Sevilla, Spain

Received 3 March 2005; accepted 27 April 2005

A series of low loading gold supported ceria/alumina catalysts have been prepared by the deposition–precipitation method, varying the pH of the synthesis. The catalysts were characterised by means of XRD, TEM, S_{BET}, XRF and UV–Vis techniques, and their catalytic activity towards CO oxidation in the absence and in presence of water in the stream, were tested. It has been found that in this low loading gold catalysts, where the metallic particles are far away one from another and the oxygen transportation is not the limiting step of the reaction, the electronic properties of the ceria phase and the structure of the metal-support perimeter more than the diameter of the gold nanoparticles is the determinant factor in the catalytic performances of the solid.

KEY WORDS: gold catalysts; CO oxidation; CeO_2/Al_2O_3 catalysts.

1. Introduction

In the last years, the use of gold supported catalysts for oxidation reactions has been widely improved [1–6]. In particular, a large number of works has focussed on the high catalytic activity of gold catalysts towards low temperature CO oxidation [7,8]. The catalytic performance of gold strongly depends on the particle size, in such a way that smaller the particles higher the activities [1]. Typically, gold particles lower than 4 nm are needed for a good activity. On the basis of this observation, most of the studies focussed on the preparation of catalyst with supported gold nanoparticles as small as possible [9, 10]. On the other hand, the nature of the support is also a key factor. In this sense it has been proved that when a reducible transition metal oxide such as Fe_2O_3 or MnO_2 is used as support, the catalytic performances of the gold catalyst for CO oxidation are improved, due to the support ability of provide reactive oxygen to the gold particles [11]. CeO_2 is one of these "active" supports, Ceria has a high oxygen storage capacity and well known catalytic and redox properties, On the other hand, it is a structural promoting component which enhances metal dispersion and participates in the stabilisation against thermal sintering of other common used supports, as alumina [12]. In a previous work we have demonstrated that CeO_2/Al_2O_3 is a suitable support for obtaining well dispersed and active gold catalyst for CO and volatile organic compounds oxidation [13,14]. The objective of this work is to demonstrate that in the case of low loading gold supported ceria/alumina catalysts, where the metallic particles are far away one from another and the oxygen transportation is not the limiting step of the reaction, the electronic properties of the ceria phase and the structure of the metal-support perimeter more than the diameter of the gold nanoparticles is the determinant factor in the catalytic performances of the solid.

*To whom correspondence should be addressed.
E-mail: centeno@icmse.csic.es

2. Experimental

2.1. Catalysts

CeO_2/Al_2O_3 supports were prepared by a son–gel method. First, 170 mL of 2-propanol was added dropwise to 17 g of $Al[(CH_3)_2CHO]_3$ (Aldrich, 98%) under continuous stirring. Afterwards, the solution was heated to 80–90 °C, maintained at such temperature for 5.5 h and cooled down to room temperature under stirring. Cerium was incorporated by gently adding to the sol a solution of 1.19 g of $Ce(NO_3)_3 \cdot 6H_2O$ (Alfa, 99.5%) in 14 mL of 2-propanol. A solution of 1.4 mL of NH_3 in 10.2 mL of H_2O was slowly added for hydrolysing the alkoxide. In such conditions, gelification takes place instantaneously. The resulting gel is dried at 40 °C for two days in an oven, and calcined for 5 h at 500 °C.

The gold containing catalysts were prepared by the deposition–precipitation method first developed by Haruta *et al.* [15]. The adequate amount of $HAuC1_4 \cdot 3H_2O$ (Alfa, 99.99% pure) was dissolved in 150 mL of deionized water and the pH of the solution adjusted around 5, 7, 9 or 11 by addition of NaOH 0.1 M. The solution was heated to 70 °C and then, the support was added and kept under continuous stirring for 1 h. In order to evaluate the effect of the temperature, one preparation was performed at room temperature. In this conditions the hydrolysis

degree of the $[AuCl_4]^-$ anion is reduced with respect to the standard conditions. The obtained solids were washed several times with deionised water in order to remove the Cl^- and Na^+ ions and dried for two days in an oven at 100 °C. Table 1 shows the code and the synthesis conditions of the studied solids.

All the prepared solids presented similar chemical composition, table 2, with only minor amounts of Si, Na and Cl. X ray fluorescence measurements stated that the concentration of Si, Na and Cl was lower than 1%, for Si, expressed as SiO_2 and less than 0.1% for sodium and chlorine.

2.2. Characterisation

BET specific surface area was measured by nitrogen adsorption liquid nitrogen temperature in a Micromeritics ASAP 2000 apparatus. Before analysis, the samples were degassed 2 h at 150 °C in vacuum.

The Ce, Al and Au contents of the samples were determined by X-ray fluorescence spectrometry (XRF) in a Siemens SRS 3000 sequential spectrophotometer with a rhodium tube as the source of radiation. XRF measurements were performed onto pressed pellets (sample included in 10 wt% of wax).

XRD analysis was performed on a Siemens D 5000 powder X-ray diffractometer. Diffraction patterns were recorded with detector-sided Ni-filtered Cu Kα radiation (40 mA, 40 kV) over a 2θ-range of 10°–60° and a position-sensitive detector using a step size of 0.05° and a step time of 1 s.

Transmission Electron Microscopy (TEM) observations were carried out in a Philips CM200 microscope operating at 200 kV. The samples were dispersed in ethanol by sonication and dropped on a copper grid coated with a carbon film.

Diffuse Reflectance UV–Vis spectra of the solids diluted in $BaSO_4$ were recorded at room temperature on a Shimadzu UV-2101PC spectrometer equipped with an integrating sphere and using $BaSO_4$ as reference. They are presented in Kubelka-Munk mode without any other transformation.

The isoeletric point (IEP) of the support was determined by measuring (Malven Zetamaster) electrophoretic mobilities of aqueous dispersions as a function of pH, at constant ionic strength (10^{-2} mol dm^{-3} NaCl). The pH was varied by adding HCl or NaOH, as needed.

Table 1
Code, Z-point and synthesis conditions of the studied solids

Code	Z-point	Synthesis			
		pH_i	pH_f	Temp (°C)	Support
CeAl1	8.14	–	–	–	–
CeAl2	8.14	–	–	–	–
AuCeAl5		5.24	7.92	70	CeAl1
AuCeAl7		7.60	7.97	70	CeAl2
AuCeAl9		9.02	8.65	70	CeAl1
AuCeAl11		11.0	10.28	70	CeAl2
AuCeAl7rt		7.05	7.56	25	CeAl1 + CeAl2

2.3. Catalytic Activity

Carbon monoxide oxidation reaction was carried out in a conventional continuous flow U-shape glass reactor (7 mm inner diameter) under atmospheric pressure. Eighty milligrams of catalyst ($\phi < 100\ \mu$ m) was placed between two plugs of glass wool and, then, the feed mixture, 84 mL/min of a reactive stream (5% Molar in CO, 5% Molar in O_2, balance He) controlled by mass flow controllers (Bronkhorst) was admitted into the reactor. In order to evaluate the influence of water in the catalytic performances of the samples, a second test was carried out in which the reactive stream was saturated with water at room temperature before the admittance into the reactor. Preliminary tests were carried out at different gas linear velocity and partial size to discard diffusional limitations. The composition of the inlet and outlet gases was analysed with a Balzers Omnistar benchtop mass spectrometer controlled by the software Balzers Quadstar 422 with capabilities for quantitative analysis. Catalytic results are measured in the steady state of reaction at the selected temperature, as deduced from the constant measurement of the CO and CO_2 concentration in the exhaust gas. The reactor showed no activity under these conditions.

3. Results and discussion

The introduction of the CeO_2/Al_2O_3 support in the gold solution resulted in a modification of the solution pH that evolves from the fixed initial one (pH_i) to a steady final value (pH_f). The difference between these two values (ΔpH) is a function of the initial pH (figure 1), by fitting this experimental data points a $\Delta pH = 0$ is obtained for a pH value equal to 8.21, extremely close to the support IEP (8.14). However, we have to take into account that our support, CeO_2/Al_2O_3, present islands of CeO_2 on the alumina surface which result in an average IEP of 8.14 but with surface patches of different IEPs.

At the pH values considered in this work the gold species present in solution are $[AuCl(OH)_3]^-$ and $[Au(OH)_4]^-$ being their relative amounts controlled by the equilibrium constant that relates then [9]. During the interaction of the gold solution with the alumina support the solution pH smoothly evolves towards the pH of the IEP of the support, figure 2, changing the relative proportion of $[AuCl(OH)_3]^-$ and $[Au(OH)_4]^-$ species and hence the interaction mechanism with the support.

Anchoring of the gold species on the support at pH below the surface IEP may result in an exchange reaction with surface hydroxyls giving rise to an increase in

Table 2
Chemical composition, BET surface area and textural properties of the studied solids

Code	Composition (% w/w)			Textural properties			
	Au	CeO_2	Al_2O_3	S_{BET} ($m^2\ g^{-1}$)	AV. Pore size (Å)	AV. pore area ($m^2\ g^{-1}$)	AV. pore volume ($cm^3\ g^{-1}$)
CeAl1	–	11.3	87.6	362.4	129.2	515.1	1.6636
CeAl2	–	11.1	88.1	387.1	131.7	545.2	1.7960
AuCeAl5	0.23	11.5	87.2	361.0	38.3	495.9	0.4747
AuCeAl7	0.37	11.0	88.0	335.8	36.6	449.9	0.4115
AuCeAl9	0.24	11.4	86.9	359.8	41.8	486.9	0.5096
AuCeAl11	0.21	11.0	87.1	289.6	37.5	375.6	0.3519
AuCeAl7rt	0.32	11.8	87.0	298.7	44.8	396.3	0.4434

the pH as experimentally observed. For pH above the surface IEP such an exchange reaction should not be possible resulting in a precipitation reaction that resulted in a decrease of the solution pH. Such acid-base equilibria may imply the modification of the support surface as a function of the solution pH and hence a possible modification of the electronic properties of the support.

The deposition–precipitation method proposed by Haruta and coworkers [3,15] is one of the most successful to obtain nanometer size supported gold catalyst. In this method the surface of the support acts a nucleating agent for the anchoring of the gold particles, being their surface properties, such as the acid/base ones, a key factor that strongly affects the final dispersion of gold. In this sense it has been proved that the average size of the obtained gold particles depends on the synthesis conditions, specially the pH. Obviously, the optimal pH changes from one support to another. In general, it seems that it is needed a pH equal or higher than the Z-point of the support for obtaining the lower particle size. Our support, a 11% w/w CeO_2/Al_2O_3 solid, has a Z point of 8.14. Thus, it is attended that preparations of gold catalyst carried out at pH higher than this value drives to gold supported particles with average size lower than the ones prepared at pH lower. Our preparation method that allows the pH of the solution to be continuosly modified may result in a broad distribution of particle sizes.

It is clear from these data that if the gold particle size depends on the interaction pH a wide distribution of diameters should be obtained in every case and, in brief we may suggest that in our case the gold particle size may be independent of the interaction pH.

The textural properties of both support and catalysts are obtained from N_2 adsorption–desorption isotherms. Figures 3 and 4 show adsorption–desorption isotherms and pore size distributions of the support and one of the catalysts, since all of them behave similarly. The isotherms correspond to typical mesoporous materials with complex pore structures made up of interconnected networks of pores of different size and shape. The gold samples are also mesoporous materials, showing a type of isotherm characteristic of ink-bottle pores which indicates that the gold particles are deposited around pores reducing their size. The surface area, pore volume

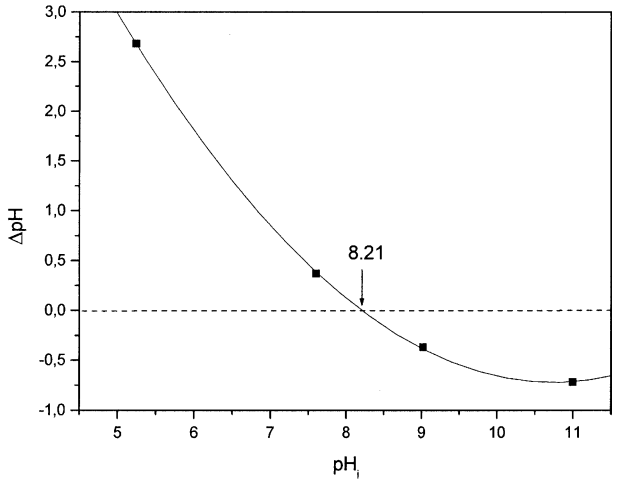

Figure 1. Incremental pH (ΔpH) between the steady final value and the fixed initial one, as a function of the later, for the considered preparations.

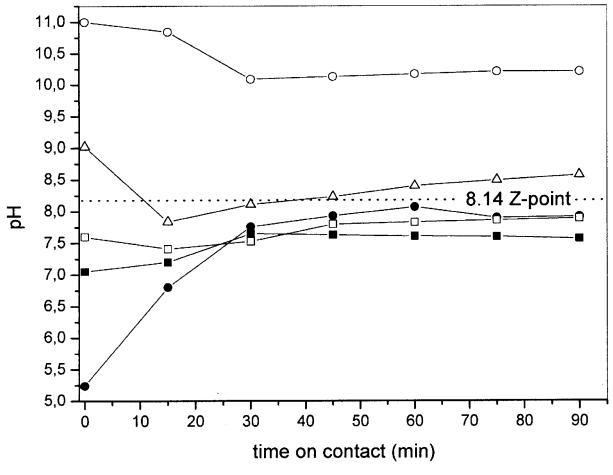

Figure 2. pH evolution during preparation of the gold samples. (●) AuCeAl5; (□) AuCeAl7; (△) AuCeAl9; (○) AuCeAl11; (■) AuCeAl7RT.

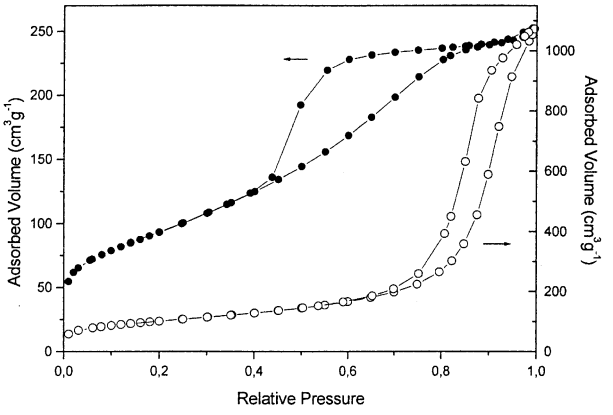

Figure 3. Typical example of the N2 adsorption–desorption isotherm of the prepared supports (◯) and gold catalysts (●).

and average pore size are independent of the pH of the solution except for the sample prepared at the higher pH and those prepared at room temperature in which case the surface area is considerably lower.

The above mentioned modification of the support surface as a function of the gold solution pH is stated by XRD measurements. In general the crystallinity of all the samples is fairly low. The diffractogram corresponding to the support only shows broad bands that can be assigned to the fluorite phase of CeO_2, (figure 5) After interaction with the gold solution two different effects can be clearly seen. First, the diffraction lines corresponding to CeO_2 become narrower and more intense which indicates particle size growth, Second, if the pH of the solution is ≥9 or the temperature is low hydrous alumina phases are evident in the diffractogram (bayerite and gibbsite). XRD diagrams are not suitable for determining Au particle size since no diffraction lines are observed except in the case of the catalyst prepared at room temperature which allows to determine that the average Au particle size is much bigger in this catalyst. Ceria particle size was calculated using the Debye

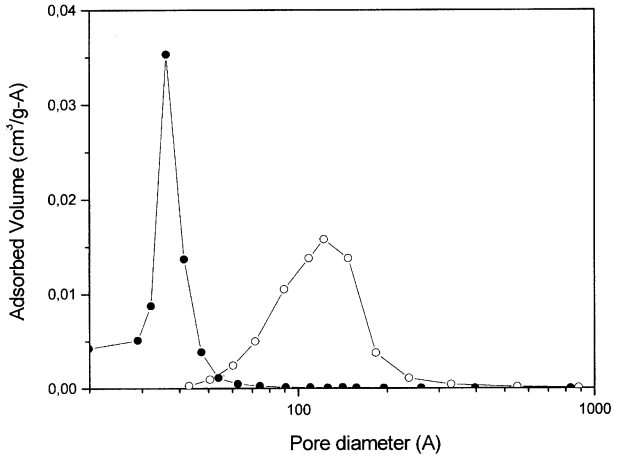

Figure 4. Typical example of the pore size distributions for the prepared supports (◯) and gold catalysts (●).

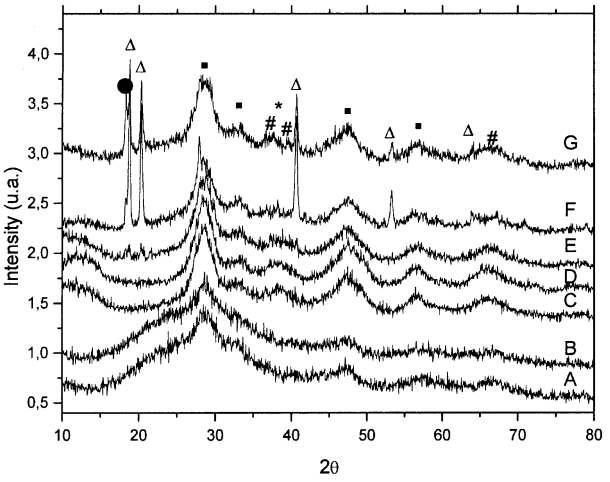

Figure 5. XRD patterns of the studied solids: (a) CeAll; (b) CeAl2; (c) AuCeAl5; (d) AuCeAl7; (e) AuCeAl9; (f) AuCeAl11; (g) AuCeAl7rt. (■), CeO_2; (#), γ-Al_2O_3; (●), $Al(OH)_3$ Gybbsite; (△), $Al(OH)_3$ Bayerite; (*), Gold).

Sherrer equation, (table 3). It can be observed the modification of the ceria particle size as a function of the initial pH of the gold solution indicating again the modification of the support surface upon interaction with the gold solution. This modification of the support surface correlates with the decrease in surface area discussed above.

The UV–Vis spectra of the considered solids are presented in figure 6. The spectrum of the CeO_2/Al_2O_3 supports present an intense absorption band with maximum at about 307 nm, which is ascribed to the overlapping of the$Ce^{4+} \leftarrow O^{2-}$ charge transfer and interband transitions, reported in pure CeO_2 at 278 and 313 nm, respectively [16, 17]. The introduction of gold in the samples induces a shift of this maximum to higher wavenumbers. The increase of the wavelength of the adsorption of a semiconductor oxide when doping with transition metal ions has been reported early in the literature and it is ascribed to the introduction of energy levels in the interband gap and implies a decrease in the band gap of the material [18,19]. The band gap of a material can be estimated from the adsorption edge wavelength of the interband transition. The most accepted method for determining the band gap energy

Table 3
CeO_2 average crystalline size of the studied solids calculated from XRD measurements

Code	CeO_2 Average crystalline size (nm)
CeAl1	3.2
CeAl2	2.1
AuCeAl5	5.1
AuCeAl7	4.3
AuCeAl9	3.6
AuCeAl11	5.2
AuCeAl7rt	5.4

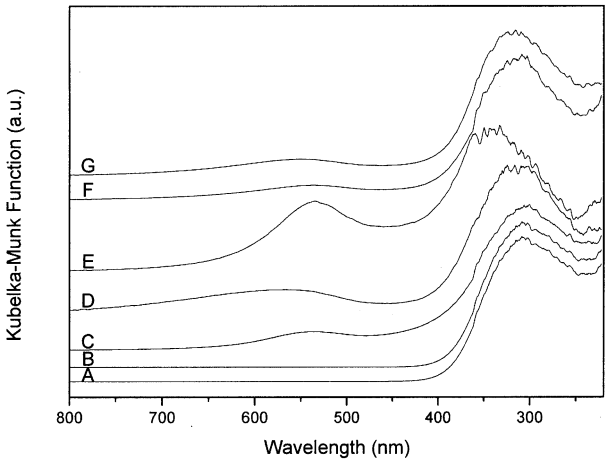

Figure 6. Diffuse Reflectance UV–Vis spectra of the studied solids: (a) CeAl1; (b) CeAl2; (c) AuCeAl5; (d) AuCeAl7; (e) AuCeAl9; (f) AuCeAl11; (g) AuCeAl7rt.

values of an insulator or semiconductor is by plotting the square root of the Kubelka-Munk function multiplied by the photon energy versus the photon energy and extrapolating the linear part of the rising curve to zero [20–22]. The results are shown in table 4. The value obtained for the support is close to that reported for CeO_2 [23] corresponding to the gap between the occupied $2p$ O band and the empty f Ce band. The band gap energy value provides evidence of the position and donating properties of the top of the valence band and can be used as a measure of the basicity of the solid [24].

As said above, the presence of gold introduces energy levels in the interband gap decreasing the band gap of the material. The band gap observed for the gold samples are different each other, thus pointing to the existence of differences in the electronic and acid/base properties among them. It has been proposed that the energy of the band gap carry information about the average crystalline domain size of the oxide (CeO_2 in our case) particles, in such a way that the domain size increase when the band gap energy decreases [16, 17], however as the measured band gap for the supported ceria particles is quite close to that measured for the bulk oxide, 3.1 eV [16, 25], it should be considered that all the observed modifications are due to the presence of gold levels being independent of the domain size of ceria particles.

In addition to the charge-transfer bands due to CeO_2, the UV–Vis spectra of the gold samples present a wide band in the 450–700 nm region which did not appear for the supports. This band is due to the surface plasmon resonance of the Au metal fine particles [26] and it is affected by the dispersed metal particle size and shape and the dielectric properties of the environment that surrounds it [27]. In our samples, a shift in the position of this band is observed from one sample to another (see table 5). However, as stated in the literature the position of the surface plasmon depends on, among others, the electric field generated by the support. As mentioned above ceria particle size change as a function of the preparation condition preventing correlations between the surface plasmon resonance and the catalytic properties of the solids.

Figure 7 shows two typical micrographs of the gold catalysts. In all samples, the gold particles are regularly distributed on the whole support, the particle size ranging from 1 to 20 nm. No clear differences in dispersion, size and shape are evidenced among the catalysts. However, we must take into account that the high atomic weight of cerium atoms in the samples makes the detection of gold particles with a very low diameter very difficult, due to the low mass and diffraction contrast. Thus, only the larger gold particles are probably detected. EDX analysis reveals that the presence of gold particles is associated with a higher concentration of cerium atoms in the surface (figures 8 and 9) which could be indicative of the participation of cerium atoms in the gold deposition process. As seen in figure 9, a significant gold content is obtained for Al/Ce atomic ratios lower than 20. This value corresponds to a 15% w/w CeO_2/Al_2O_3 composition. Thus, it seems that, in CeO_2/Al_2O_3 systems, gold is deposited preferentially over the ceria phase, or in surface places where a local concentration of CeO_2 is at least of 15% w/w. A similar conclusion was deduced in a previous work from XPS results [13]. Recently it has been reported that when the gold deposition–precipitation process is carried out on a titanium oxynitride support where a TiO_2 and a TiN phase coexist, gold is selectively deposited on the oxide

Table 4
Band gap energy of the studied solids, calculated from DR–UV–Vis measurements

Code	Band gap energy value (eV)
CeAl1	2.92
CeAl2	3.00
AuCeAl5	2.50
AuCeAl7	2.69
AuCeAl9	2.44
AuCeAl11	2.78
AuCeAl7rt	2.81

Table 5
Experimental position of the DR–UV–Vis surface plasmon resonance band of gold particles for the studied gold catalysts

Code	Position (nm)
CeAl1	–
CeAl2	–
AuCeAl5	537
AuCeAl7	570
AuCeAl9	535
AuCeAl11	539
AuCeAl7rt	551

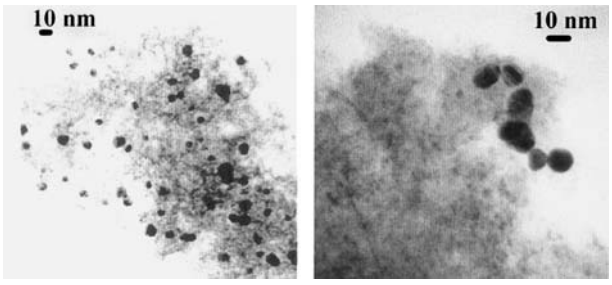

Figure 7. Typical TEM micrographs of catalysts.

particles, showing that the acid-base properties of the support play a decisive role in the success of the gold deposition process [10]. From here, the preferential precipitation of gold over the ceria phase can be explained by the more basic character of CeO_2 compared to alumina. In fact, it has been described that when cerium is in direct contact with alumina, Ce-bound oxide ions are more basic than aluminate-type ligands since Ce is less electronegative than Al [28,29].

Figure 10 shows the CO conversion as function of temperature on the considered catalysts in dry and wet conditions. $CeO_2/Al2O_3$ supports themselves begin to be active at temperatures higher than 300 °C, The support is slightly active at high temperatures reaching a 80% CO conversion at 450 °C in the absence of water in the reactive stream, The introduction of gold strongly enhances the activity of the samples. Due to the low gold content of the samples, the activity is not extremely high, achieving a complete CO conversion at 220 °C in the most active situation (AuCeAl7rt, dry conditions). The influence of the presence of water in the reactive stream can be observed in figure 11. At temperatures lower than 120 °C water exerts a positive influence in the catalyst's activity, however, above this temperature the water effect becomes negative. In order to compare the activity performances of the catalysts, the temperature

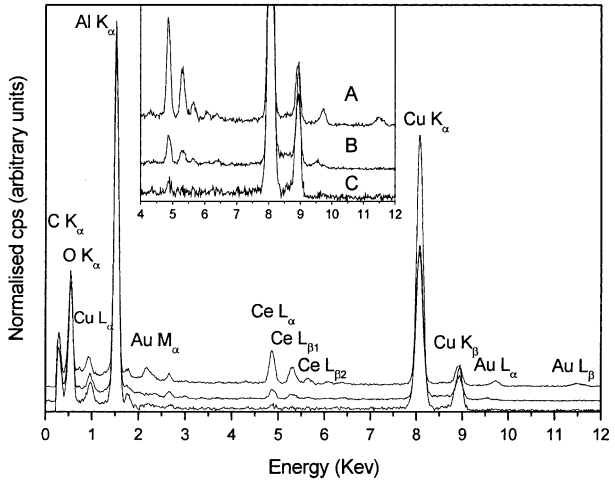

Figure 8. Typical EDX analysis of gold samples.

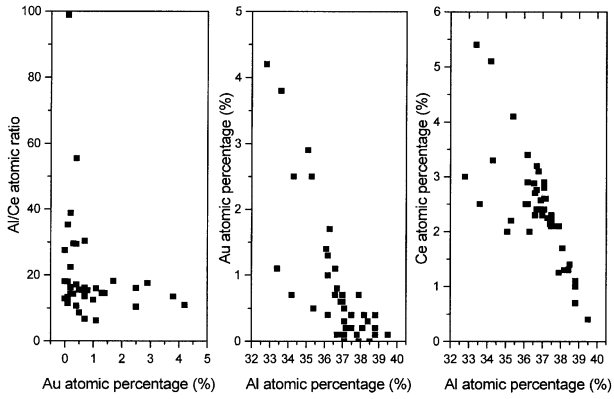

Figure 9. Some experimental EDX relationships obtained for the studied gold catalysts.

at which the 50% of the initial CO is converted into CO_2 (T_{50}) is presented in table 6.

On the other hand, the surface and electronic properties of the support used have resulted determinant in the final surface and catalytic properties of the obtained gold catalysts. In this sense, the UV–Vis results are very illustrative. The band gap in CeO_2 represents the difference in energy between the O^{2-} and the Ce^{4+} levels. As said in the results section, the presence of gold

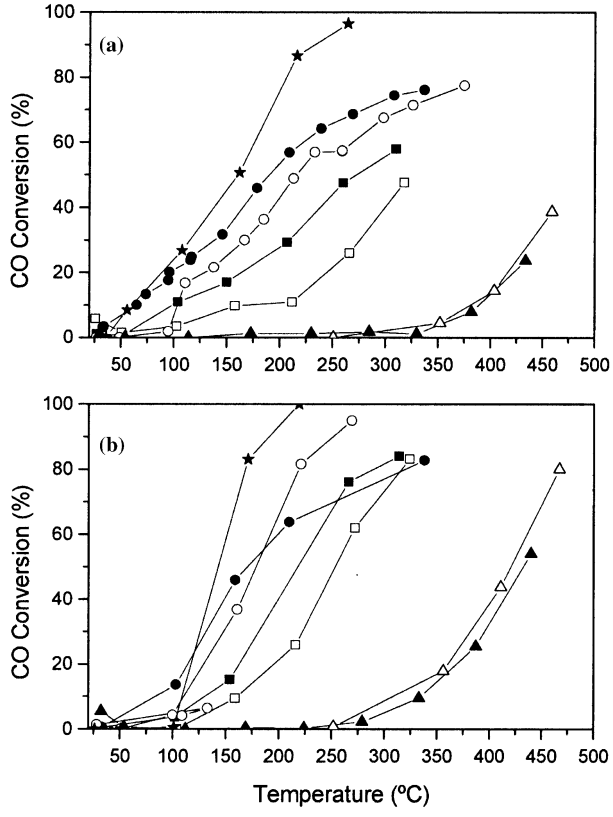

Figure 10. CO conversion for the studied catalysts, as a function of temperature, in wet (a) and dry (b) conditions. (■) AuCeAl5; (●) AuCeAl7; (□) AuCeAl9; (○) AuCeAl11; (*) AuCeAl7RT; (▲) CeAll; (△) CeAl2.

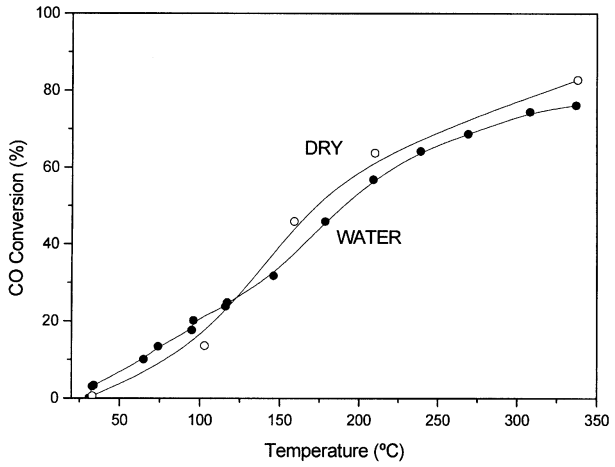

Figure 11. Influence in the CO conversion, as a function of temperature, of the presence of water in the feed on AuCeAl7.

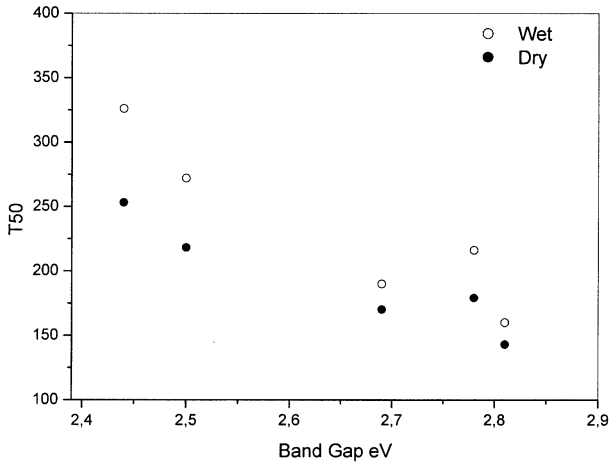

Figure 12. Relationship between the activity towards CO oxidation and the band gap of the gold samples.

introduces energy levels in the interband gap decreasing the band gap of the material. The band gap measured in gold samples is therefore the difference in energy between the gold and the Ce^{4+} levels. The catalytic activity to CO oxidation of the samples is a function of this band gap, (figure 12), in such a way that the higher band gap the higher the activity. This behaviour can be interpreted in terms of separation between energy levels, showing that the higher catalytic activity is obtained when the energy levels introduced by gold are closer to the O^{2-} ones, (figure 13), that means, when the easiness of the electron transfer between oxygen atoms of ceria and gold is higher. This observation indicates that the interface between ceria and gold particles is a key factor to explain the activity of $Au/CeO_2/Al_2O_3$ catalysts in the CO oxidation reaction, which agrees with the preferential deposition of gold over the ceria phase of the support. On the other hand, most of the literature data agree with the assumption that CO oxidation reaction over gold supported samples takes place between CO molecules adsorbed on gold particles and oxygen molecules adsorbed at the interface with the support [30,31]. In the case of Au/CeO_2 catalysts, the reaction sites have been described to be placed at the borderline of the small gold particles on the surface of defective ceria [31].

Table 6
Activity of the studied gold samples in the CO oxidation reaction. Temperature at which the 50% of the initial CO is converted into CO_2 (T_{50})

Code	Wet Conditions T_{50} (°C)	Dry Conditions T_{50} (°C)
CeAl1	521	432
CeAl2	484	420
AuCeAl5	272	218
AuCeAl7	190	170
AuCeAl9	326	253
AuCeAl11	216	179
AuCeAl7rt	160	143

The oxidation state of reactive gold species is also a topic under discussion, Metallic gold are generally the considered active species for oxidation reactions [7, 30], although oxidized ones have been also proposed to contribute [13,32, 33]. Even $Au^{\delta-}$ sites have been also describe as active centers at the beginning of the water gas shift reaction over Au/CeO_2 catalysts [31]. Our observation of the higher activity of the gold/ceria samples with the lower gold to oxygen energy levels separation implies a predominant role of the $Au^{\delta+}$ species. The role of the ceria phase is to control and maintain the adequate oxidation state of gold active sites and enhance the lattice oxygen mobility. In this sense it is well known the high oxygen storage capacity of ceria due to their redox properties associated to the fast reduction/oxidation cycles $CeO_2 \leftrightarrow Ce_2O_3$. It is recently established that in the presence of gold the reducibility of ceria is enhanced [31]. The same authors proposed that on Au/CeO_2 catalysts, CO is adsorbed on

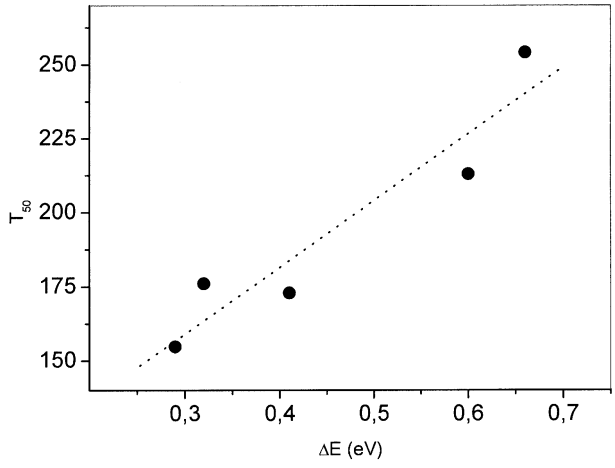

Figure 13. Relationship between the activity towards CO oxidation and the separation in energy between the gold and the O^{2-} levels, for the studied gold samples.

gold step sites close to the support and Ce^{3+} centers, which when reoxidate produce oxygen molecules which dissociates in adsorbed atomic oxygen and react with CO to give CO_2. On the other hand, water is able to reoxidize reduced ceria at room temperature [31,34]. From here, the observed positive effect of the presence of water in the CO oxidation activity of the samples at temperatures lower than 120 °C (figure 11) can be ascribed to the improved of the control of the redox reactions implied in the reaction mechanism of the catalytic system, favouring a more oxidation degree of ceria. Above 120 °C, the effect of water in the CO oxidation reaction becomes negative, According to Padeste *et al* [34], the efficiency of water to reoxidize reduced ceria is maintained at elevated temperature (at least 550 °C), even with low partial pressures of H_2O. On the other hand, the oxygen mobility is increased with temperature by thermal activation, such leading to the enhanced catalytic activity of the system. In such conditions, the oxidative properties of water can shift the $Ce^{4+} \leftrightarrow Ce^{3+}$ equlibrium to the left, decreasing the amount of Ce^{3+} and the speed of the oxidation/reduction ceria cycles which imply a lower oxygen storage capacity, and a decrease in the CO oxidation activity. Our results agree with the ones of Fu *et al.* [33], which found a correlation between the high catalytic activity of their gold-ceria catalysts for low-temperature water–gas shift reaction and the ceria structure and the oxygen transfer properties of the solids.

The catalytic activity of the samples also correlates with the position in the UV–Vis spectra of the surface plasmon resonance band of gold particles, (figure 14). The position of this band is affected by the dispersed metal particle size and shape and the dielectric properties of the environment. As already stated, we have a no direct measurement of the gold particle size in the samples although indirect ones make us think that it would increase when decreasing the pH of the synthesis. if it so, figures 10 and 12 shows that the catalytic activity does not correlate with the gold particle size. Then, we can assume that electronic properties of the environment are the determinant factor in the activity and, probably, in the observed shift of the gold plasmon band.

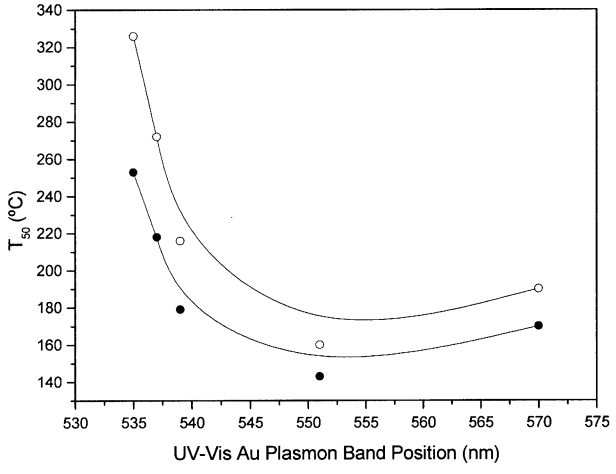

Figure 14. Relationship between the activity towards CO oxidation and the experimental position of the DR–UV–Vis surface plasmon resonance band of gold particles.

4. Conclusions

We have prepared a series of low loading (*circa* 0.3% w/w) gold supported ceria/alumina catalysts by the deposition–precipitation method, varying the pH of the synthesis, from 5 to 11. In all cases, gold is preferentially deposited onto the ceria phase, as deduced from EDX analysis. The catalytic activity to CO oxidation of the gold samples is a function of the measured band gap, which is the difference in energy between the gold and the Ce^{4+} levels, in such a way that the higher catalytic activity is obtained when the energy levels introduced by gold are closer to the O^{2-} ones, that means, when the easiness of the electron transfer between oxygen atoms of ceria and gold is higher. From here, the key role of the interface between ceria and gold particles in the activity of $Au/CeO_2/Al_2O_3$ catalysts in the CO oxidation reaction, is deduced. In these low loading gold samples, the electronic properties of the ceria phase and the structure of the metal-support perimeter are more determinant than the diameter of the gold nanoparticles in the catalytic performances of the solid.

On the other hand, the observed positive effect of the presence of water in the CO oxidation activity of the samples at temperatures lower than 120 °C can be ascribed to the improved of the control of the redox reactions implied in the reaction mechanism of the catalytic system, favouring a more oxidation degree of ceria

Acknowledgements

The financial support by the Spanish Minsterio de Ciencia y Tecnología, MCYT (REN2000-0517 and MAT2003-06540-CO2) is gratefully appreciated.

References

[1] G.C. Bond and D.T. Thompson, Catal. Rev.-Sci. Eng. 41 (1999) 319.
[2] G.J. Hutchings, Gold. Bullet. 37 (2004) 3.
[3] M. Haruta, Catal. Today 36 (1997) 153.
[4] V. Idakiev, T. Tabakova, Z.-Y. Yuan and B. Su, Appl. Catal. A 270 (2004) 135.
[5] Y. Tai, J. Murakami, K. Tajiri, F. Ohashi, M. Daté and S. Tsubota, Appl. Catal. A 268 (2004) 183.
[6] D. Andreeva, R. Nedyalkova, L. Ilieva and M.V. Abrashev, Appl. Catal. B 52 (2004) 157.
[7] L. Guczi, D. Horvath, Z. Paszti and G. Peto, Catal. Today 72 (2002) 101.

[8] M. Olea and Y. Iwasawa, Appl. Catal. A 275 (2004) 35.
[9] S. Ivanova, C. Petit and V. Pitchon, Appl. Catal. A 267 (2004) 191.
[10] M.A. Centeno, I. Carrizosa and J.A. Odriozola, Appl. Catal. A 246 (2003) 365.
[11] M.M. Schubert, S. Hackemberg, A.C. Veen, M. Muhler, V. Plzak and R.J. Behm, J. Catal. 197 (2001) 113.
[12] A. Martinez-Arias, M. Fernandez-Garcia, L.N. Salamanca, R.X. Valenzuela, J.C. Conesa and J. Soria, J. Phys. Chem. B 104 (2000) 4038.
[13] M.A. Centeno, M. Paulis, M. Montes and J.A. Odriozola, Appl. Catal. A 234 (2002) 65.
[14] M.A. Centeno, M.I. Domínguez, I. Carrizosa, J.A. Odriozola, Proceedings of the XVIII Iberoamerican Symposium on Catalysis (2002), p. 2640.
[15] S. Tsubota, D.A. Cunningham, Y. Bando, M. Haruta, in: G. Poncelet, P. Grange and P.A. Jacobs (eds)., Preparation of Catalysts VI, Elsevier, Amsterdam, 1995, p. 227..
[16] M.I. Zaki, G.A.M. Hussein, S.A.A. Manssur, H.M. Ismael and G.A.H. Mekhemer, Colloids and Surfaces A 127 (1997) 47.
[17] A. Bensalem, J.C. Muller and F. Bozon-Verduraz, J. Chem. Soc. Faraday Trans. 88 (1992) 153.
[18] J.A. Navio, M.C. Hidalgo, G. Colón, S.G. Botta and M.I. Litter, Langmuir 17 (2001) 202.
[19] G.R. Rao and H.R. Sahu, Proc. Indian. Acad. Sci. (Chem. Sci.) 113 (2001) 651.
[20] S.P. Tandom and J.P. Gupta, Phys. Stat. Sol. 38 (1970) 363.
[21] R.S. Weber, J. Catal. 151 (1995) 470.
[22] D.G. Barton, M. Shtein, R.D. Wilson, S.L. Soled and E. Iglesia, J. Phys. Chem. B 103 (1999) 630.
[23] N.V. Skorodumova, R. Ahuja, S.I. Simak, I.A. Abrikosov B. Johansson and B.I. Lundqvist, Phys. Review B 64 (2001) 115108.
[24] M.A. Centeno, M.J. Capitán, P. Malet, I. Carrizosa and J.A. Odriozola, J. Catal. 148 (1994) 399.
[25] K.B. Sundaram and P. Wahid, Phys. Rev. B 161 (1990) 163.
[26] P. Mulvaey, Langmuir 12 (1996) 788.
[27] P. Bera and M.S. Hedge, Catal. Lett. 79 (2002) 107.
[28] J. Soria, J.M. Coronado and J.C. Conesa, J. Chem. Soc. Faraday Trans 92 (1996) 1619.
[29] C. Morterra, V. Bolis and G. Magnacca, J. Chem. Soc. Faraday Trans. 92 (1996) 1991.
[30] M. Haruta and M. Date, Appl. Catal. A 222 (2001) 427.
[31] T. Tabakova, F. Bocuzzi, M. Manzini and D. Andreeva, Appl. Catal. A 252 (2003) 385.
[32] G.C. Bond and D.T. Thompson, Gold Bull. 33 (2000) 41.
[33] Q. Fu, S. Kudriavtseva, H. Satsburg and M. Flytzani-Stephanopoulus, Chem. Eng. J. 93 (2003) 41.
[34] C. Padeste, N. Cant and D. Trimm, Catal. Lett. 18 (1993) 305.
[35] S. Deki, Y. Aoi, H. Yanagimoto, K. Ishii, K. Akamatsu, M. Mizuhata and A. Kajinami, J. Mater. Chem. 6 (1996) 1879.